UNIVERSITY OF OKLAHOMA

GRADUATE COLLEGE

HOMER L. DODGE DEPARTMENT OF PHYSICS AND ASTRONOMY

THE MUON ANOMALOUS MAGNETIC MOMENT: A PROBE FOR THE STANDARD MODEL AND BEYOND

A REPORT

SUBMITTED TO THE GRADUATE FACULTY

in partial fulfillment of the requirements for the

SPECIALIST'S EXAMINATION

By

OTHMANE RIFKI
Norman, Oklahoma
2014

THE MUON ANOMALOUS MAGNETIC MOMENT: A PROBE FOR THE STANDARD MODEL AND BEYOND

A REPORT APPROVED FOR THE
HOMER L. DODGE DEPARTMENT OF PHYSICS AND ASTRONOMY

BY

Dr. Brad Abbott, Chair

Dr. S. Lakshmivarahan, Outside Member

Dr. Mike Strauss

Dr. Chung Kao

Dr. Eric Abraham

Table of Contents

List of Tables

List of Figures

Abstract

The muon is a spin-$\frac{1}{2}$ charged particle characterized by an intrinsic magnetic moment with a *gyromagnetic ratio*, g, that is very close to 2. Its departure from 2 is referred to as the magnetic moment anomaly $a_\mu = \frac{g-2}{2}$ that has been determined over the last decades to ever higher precisions in both experiment and theory. The most recent experiment (E821) was performed at Brookhaven National Laboratory and achieved a precision of 0.54 ppm, while the current theoretical evaluation stands at a precision of 0.39 ppm. However, the experimental value is higher than the predicted value by more than 3 standard deviations which suggests the possibility of new physics. A new experiment (E989) is being built at Fermi National Laboratory to investigate the discrepancy by reducing the experimental error to 0.14 ppm. In parallel, theory groups are working to reduce the error in a_μ to match the projected experimental precision. A confirmation of the difference between experiment and theory will have an impact on new physics models in the TeV scale. The goal of this review is to describe the E821 measurement of a_μ, the improvements implemented in E989, the current theoretical status in the computation of a_μ, and the new physics implications.

The closer you look the more there is to see

Friedrich Jegerlehner, *The Anomalous Magnetic Moment of the Muon* [1].

1 Introduction

The study of elementary particles and their interactions led to a representative mathematical formulation known as the *Standard Model* (SM) of particle physics. When subjected to experimental tests, the SM successfully describes three of the four fundamental forces: electromagnetic, weak, and strong interactions. On the other hand, the SM is not believed to be complete since it fails to explain a number of problems that are still facing today's physics community. First, the SM does not incorporate the fourth fundamental force of gravity. Moreover, It does not provide insight on the nature of the "invisible" matter that is holding galaxies together, which constitutes $\sim 26\%$ of the energy density of the universe and is known as *Dark Matter*. Few other examples are the different masses and mixing of the 12 leptons known as the *flavor problem*, and the predominance of matter over antimatter. In order to solve these problems, searches for physics not incorporated in the SM have been pursued in both experiment and theory. Any sign of significant discrepancy between experiment and theory is taken very seriously since it might lead to new insights that can reveal what is missing in our current view of the universe. Some experiments have looked for answers to SM problems by studying high energy interactions as is pursued at the Large Hadron Collider at CERN, in the hope of observing some new particles. This

led to the discovery of the Higgs boson in 2012, a central piece of the SM. Other experiments have performed detailed studies of known particles by measuring their properties to very high precisions and comparing them to theoretical calculations to both check the models and look for discrepancies. The subject of this current review is an important illustration of the latter scenario where precision tests of the intrinsic property of a spinning charged elementary particle known as the *magnetic moment* will be examined by comparing experiment to theory.

The possible elementary charged particles that can be used to measure the magnetic moment are the three spin $\frac{1}{2}$ leptons: the electron e, the muon μ, and the tau τ. While these particles have the same charge and spin, they have very different masses which are given by[1] $m_e = 0.511$ MeV/c^2, $m_\mu = 105.658$ MeV/c^2, and $m_\tau = 1776.82$ MeV/c^2. The difference in masses alters the lifetimes and decay modes of each particle. The electron is the lowest mass charged lepton and thus is stable; the muon lifetime is $\tau_\mu = 2.197 \times 10^{-6}$ seconds and it decays almost 100% to an electron and two neutrinos ($e\nu_\mu\bar{\nu_e}$); while taus have a much shorter lifetime $\tau_\tau = 2.906 \times 10^{-13}$ seconds and a diversified decay pattern where 65% go into hadronic states (states that contain quark-antiquark pair particles such as pions) and the remainder go into leptonic states (the two possible states are muons and two neutrinos or electrons and two neutrinos) [2]. Because of its very short lifetime, the study of the tau's magnetic moment is not possible using the current technology, leaving the electron and the muon as the appropriate candidates. While the electron is the most precisely studied lepton, effects in the

[1]The unit of mass is given in MeV/c^2 according to the relation $E = mc^2$ with the energy E given in units of MeV where 1 MeV = 1.6×10^{-13}J.

magnetic moment sensitive to physics beyond the SM scale with powers of m_ℓ^2 [3]. For this reason, muons are more appropriate for the study of the magnetic moment to search for new physics. The magnetic moment arises from the electric charge and the current of an elementary particle with spin. For instance, a classical calculation of a particle with mass m, and charge q, moving in a circular orbit of radius r, with velocity $\overrightarrow{v}$, shows that its magnetic moment $\overrightarrow{\mu}$ is related to its orbital angular momentum ($\overrightarrow{L} = m\overrightarrow{r} \times \overrightarrow{v}$) by the relation:

$$\overrightarrow{\mu} = \frac{q}{2mc}\overrightarrow{L} \tag{1}$$

(see Appendix A). In quantum mechanics, the magnetic moment is an intrinsic property of a particle with spin. Both the magnetic moment and the orbital angular momentum are promoted to operators in order to give the correct quantum mechanical representation. While Equation (1) is still valid in describing the orbital angular momentum $\overrightarrow{L}$, the spin magnetic moment requires a modification by a factor g that is very close to 2. The corrected equation is given by

$$\overrightarrow{\mu} = g\frac{q}{2mc}\overrightarrow{S}, \tag{2}$$

where g is called the *gyromagnetic ratio* or *g-factor*, and q is the charge given in units of the fundamental charge e where $q = -e$ for a lepton particle (negative muon) and $q = +e$ for a lepton antiparticle (positive muon). $\overrightarrow{S}$ is the *spin operator*

$$\overrightarrow{S} = \frac{\hbar}{2}\overrightarrow{\sigma}, \tag{3}$$

where σ_i are the Pauli spin matrices. The result $g = 2$ was first obtained by Dirac in 1928 when he generalized the Schröedinger equation to incorporate

special relativity. With the development of the quantum mechanical description of electromagnetism known as quantum electrodynamics (QED), g was found to differ from 2 by an anomaly a_ℓ, known as the *magnetic moment anomaly*, or the *anomaly* for short, such that: $g_\ell = 2(1 + a_\ell)$. The anomaly is then

$$a_\ell = \frac{g_\ell - 2}{2}. \tag{4}$$

The $g-2$ factor appeared! This is the title of all experiments that measure the magnetic moment of the muon and it is the focus of this review.

In addition to the quantum fluctuations of the electromagnetic field described by QED, quantum fluctuations due to heavier particles such as the weak gauge bosons ($W^{\pm}$ and Z bosons) and hadrons (for example quark-antiquark pairs such as pions) also contribute to the anomaly. These effects are known as radiative corrections (RC) and are mainly dominated by QED as it will be discussed in Section 5. The anomaly scales as $\delta a_\ell \sim \frac{m_\ell^2}{M^2}$ where $M \gg m_\ell$ can represent the mass of a heavier SM particle, the mass of an unobserved heavy particle beyond the SM, or an energy range where the SM is no longer valid [3]. From this relation, we first see that a_μ is more sensitive to new effects than a_e by a factor of $(m_\mu/m_e)^2 \approx 4 \times 10^4$. On the other hand, heavier states (large M) have smaller effects ($\sim 1/M^2$) which places the determination of $g-2$ as a good probe for interactions with energies at the TeV scale. The LHC is currently probing the TeV energy scale, so $g-2$ will complement and guide the LHC searches and may even be more sensitive to new physics that is not accessible to the LHC.

The importance of $g-2$ is in the fact that it can be precisely measured as

it will be discussed in Section 3 and it can be precisely calculated based on all RC of the SM as it will be discussed in Section 5. On the experimental side, the most recent experiment is the Brookhaven National Laboratory (BNL) E821 $g-2$ experiment that concluded its run in 2001, with a final reported result of [4]:

$$a_\mu^{\text{E821}} = (116\,592\,08.0 \pm 6.3) \times 10^{-10}\,(0.54\text{ ppm})\,[4], \tag{5}$$

where ppm refers to the precision in parts per million given by the ratio of the total error to the value as σ_X/X. The anomaly has been evaluated by different groups. One of its recent calculations is

$$a_\mu^{SM} = (116\,591\,82.8 \pm 4.5) \times 10^{-10}\,(0.39\text{ ppm})\;\;[5], \tag{6}$$

which gives a difference of

$$\Delta a_\mu\,(\text{E821} - \text{SM}) = (25.2 \pm 7.7) \times 10^{-10}. \tag{7}$$

The difference between the measurement and the prediction is 3.3 standard deviations with the measurement having the higher value. In particle physics, a three standard deviation effect "3σ" means that the probability of the measurement to randomly fluctuate from the predicted value by 3σ is equivalent to the probability of obtaining a value on a Gaussian distribution that is at least 3 standard deviations away from the expected mean. This corresponds to a probability of 1.35×10^{-3} (on average 1 out of every 740 measurements). In order to be confident that the difference is not just a statistical fluctuation, a difference of five standard deviations "5σ" is required, which implies that the probability of such variation is 3×10^{-7} (on average 1 out of every 3.5 million measurements).

A separate independent experiment is designed to reduce the error in Equation (5) to $\sim 1.6 \times 10^{-10}$ giving a precision of 0.14 ppm with a four-fold improvement over the BNL result [4]. Assuming that a similar value for the anomaly is obtained and the theoretical calculation is exactly the same, the new deviation is 5.3σ, which will confirm the discrepancy. This new experiment is currently being built at Fermi National Laboratory (FNAL) under the name E989 Muon $g-2$ Experiment. An error improvement in the measurement of $g-2$ implies that the error in the calculated prediction should also be improved to the same level. In the event that E989 confirms this discrepancy, a door for an extension of the SM will be open for new theoretical models such as supersymmetry[2], extra dimensions[3], or a dark matter particle.

This review will describe the experimental technique used to measure the anomaly and present the status of the theoretical calculations. It will also address the future improvements in both areas and conclude with new physics possibilities.

2 The Muon Properties

The muon anomaly can be measured to ppm precision by studying the behavior of the spin magnetic moment of muons in circular orbits subjected to a uniform magnetic field. In this section, the key ideas that permit the measurement will be introduced to lead up to a discussion of the BNL experiment in the next section.

[2]Supersymmetry (SUSY) theory postulates that a space-time symmetry exists between the two classes of the SM elementary particles: fermions and boson. It incorporates the four fundamental forces and predicts energy interactions beyond the weak scale. However, experimental evidence has yet to support the theory.

[3]Extra dimension models postulate the existence of dimensions other than the three spatial dimensions and the temporal dimension.

2.1 Obtaining Polarized Muons

Muons are obtained from pions that are acquired from sending a high intensity beam of protons into a target material that has the property of being resistant to high stresses, nickel for example. The decay of positive and negative pions produces positive and negative muons according to

$$\begin{aligned} \pi^+ &\rightarrow \mu^+ + \nu_\mu, \\ \pi^- &\rightarrow \mu^- + \overline{\nu}_\mu. \end{aligned} \tag{8}$$

The spin orientation, called *polarization*, of the decayed muon is well determined for the cases of positive and negative pions. This can be seen by introducing the concepts of *helicity*, *parity transformation*, and *charge conjugation*. Helicity is defined as the projection of spin $\overrightarrow{S}$ along the momentum direction $\hat{p} = \overrightarrow{p}/|\overrightarrow{p}|$ such that $h = \overrightarrow{S} \cdot \hat{p}$. For a spin-$\frac{1}{2}$ particle, it is right-handed when $h = +1/2$ (spin and momentum parallel) and left-handed when $h = -1/2$ (spin and momentum anti-parallel). Parity, represented by the operator P, creates the mirror image of a physical process. For example, for a vector $\overrightarrow{x}$, $P\,|\overrightarrow{x}\rangle = -\,|\overrightarrow{x}\rangle$. Charge conjugation, represented by the operator C, refers to the conversion of a particle to its antiparticle by changing the sign of all its quantum numbers (electric charge, lepton number, baryon number, and flavor charges such as strangeness).

By starting from a spin zero pion and a right-handed antineutrino, the possible transformations are C, P, or both CP as shown in Figure 1. Experimental evidence shows that neutrinos can only be left-handed and antineutrinos can only be right-handed. For this reason, the only possible process is the one obtained

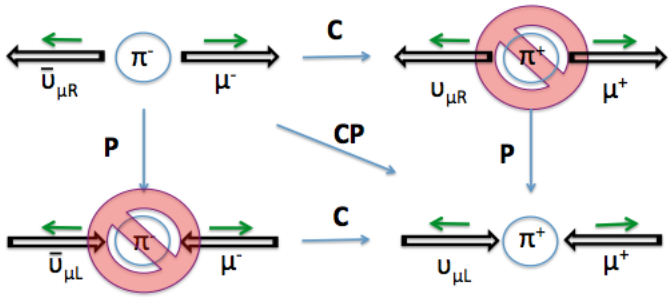

Figure 1: An illustration of the possible decays of a pion. The black arrow represents the spin vector and the green arrow represents the momentum orientation.

by a CP transformation, which makes a negative pion produce a right-handed negative muon ($h = +1/2$), and a positive pion produce a left-handed positive muon ($h = -1/2$).

2.2 Parity Violation

While parity is a conserved quantity in electromagnetic and strong interactions, it is not conserved in the weak interactions. In fact, the muon weak decays

$$\begin{aligned} \mu^- &\rightarrow e^- + \overline{\nu}_e + \nu_\mu, \\ \mu^+ &\rightarrow e^+ + \nu_e + \overline{\nu}_\mu \end{aligned} \tag{9}$$

are parity violating events, which means that the emitted electrons[4] have a favored direction of emission. Because of parity violation in weak processes, a correlation exists between the momentum direction of the decaying electron and the spin orientation of the muon. In other words, there is a preferred direction for the decay of the electron for each spin orientation of the muon. For an illustration of

[4]Unless specified, electron refers to both the electron and its antiparticle, the positron.

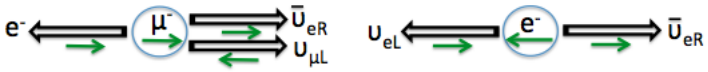

Figure 2: In the laboratory frame, the muon spin and momentum are parallel and directed to the right. Both decays are in the MRF and show the more likely electron direction. The left decay shows an electron having the maximum possible energy $E_{e,\max} \sim \left(m_\mu c^2\right)/2 =$ 53 MeV. The right decay shows an electron emitted at rest with its spin antiparallel to its laboratory momentum.

this correlation, the negative muon decay is considered in the two limiting cases of Figure 2 in the muon rest frame (MRF). Note that the muon momentum and spin are parallel and directed to the right in the laboratory frame to better understand the spin and momentum orientations of the right figure.

If the electron has the maximum possible energy in the MRF, the two neutrinos will be emitted back-to-back to the electron with the latter carrying approximately half of the rest mass energy of the muon in order to conserve momentum, $E_{e,\max} \approx \left(m_\mu c^2\right)/2 = 53$ MeV [5]. Parity violation favors the electron to be emitted left-handed which implies that its momentum will be anti-parallel to the muon spin as shown in the left figure. In the case of a zero momentum electron in the MRF, the neutrino and antineutrino will be emitted antiparallel to each other with their spins parallel. Since the electron has a preferred spin direction antiparallel to the muon laboratory momentum, and the muon momentum and spin are parallel.

[5]More precisely, the conservation of energy leads to $E_{e,\max} = \dfrac{m_\mu^2 + m_e^2}{2m_\mu} c^2$. The above approximation holds when the value $\dfrac{m_e c^2}{E_{e,\max}} = 9.6 \times 10^{-3}$ is negligible.

The electron will be emitted parallel to the muon spin as shown on the right figure. These two examples show that by knowing the direction of the decay electron, the muon spin orientation can be inferred. This is the key idea of the muon $g-2$ measurement. By placing muons with the same polarization in a circular orbit with a uniform magnetic field, their spin component parallel to the momentum vector, longitudinal polarization, will change slightly with each orbit at a rate that is directly related to the anomaly $a_\ell = \frac{g_\ell - 2}{2}$. The change in the muon longitudinal polarization is determined by using the asymmetric angular distribution of the decay electrons. Formally, the differential decay probability for an electron to be emitted with a normalized energy $y = E/E_{e,max}$ at an angle θ with respect to the muon spin is given in the MRF with the approximation $E_e \gg m_e c^2$ by

$$dP^{\pm} \propto N\left(E_e\right)\left(1 \pm A(E_e)\cos\theta\right) dy d\Omega, \tag{10}$$

where the $(+)$ is for positive muons decay and the $(-)$ is for negative muons decay and $d\Omega$ is the solid angle. $N\left(E_e\right)$ is a normalization factor that represents the number of decay electrons per unit energy and $A\left(E_e\right)$ is the non-vanishing coefficient of $\cos\theta$ which represents the decay asymmetry factor that reflects the *parity violation*. The expressions of $N\left(E_e\right)$ and $A\left(E_e\right)$ are given by

$$N\left(E_e\right) = 2y^2\left(3-2y\right) \text{ and } A\left(E_e\right) = \frac{1-2y}{3-2y}. \tag{11}$$

These relations are derived in Appendix B.

A few remarks related to equations 10 and 11 are in order. First, the number of decay electrons and asymmetry reach their highest values in the MRF when the energy of the emitted electron is maximum ($y = 1$) as shown in Figure 3.

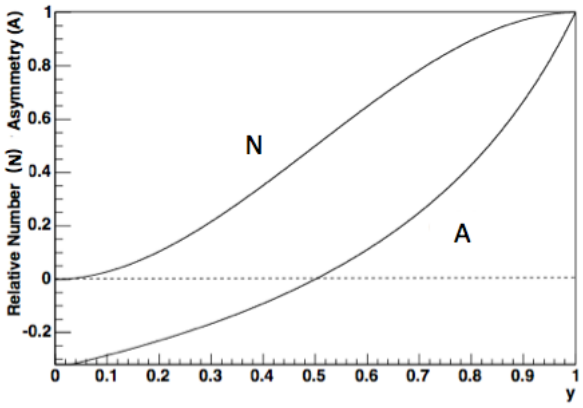

Figure 3: The number of decay electrons and the asymmetry distributions in the MRF as a function of the fractional energy $y = E/E_{e,max}$ [4].

Also, the asymmetry changes sign at half the maximum energy ($y = \frac{1}{2}$) which means that the emitted electron will have a preferred handedness (or helicity) based on its energy. More importantly, the probability of emitting a specific number of electrons varies with the angle θ between the electron and the muon spin directions. To be precise, there are more high energy electrons (e^-) emitted when their momenta are anti-parallel to the muon (μ^-) spins than when they are parallel. By only selecting the highest energy electrons and counting their number, the spin direction of the muons can be inferred: when the number of electrons is maximum, the muon spin is anti-parallel to the emitted electron direction, and when the number is minimum, the muon spin is parallel to the emitted electron direction. A similar reasoning can be followed for high energy positrons (e^+) which will reach a maximum number when the positive muon (μ^+) spins are parallel to the emitted positrons. If the spin of the muons is allowed to precess, then the

number of high energy electrons will also precess at the same rate, allowing a direct measurement of the precession frequency.

2.3 Relativistic Muons in a Magnetic Field

In classical electromagnetism, the effect of a uniform magnetic field on a bar magnet is to exert a torque that will align the magnet with the magnetic field. However, if the magnet is spinning, then conservation of angular momentum will cause the bar magnet to precess around the magnetic field. Similarly, the muon has an intrinsic spin and an intrinsic magnetic moment. The interaction of the muon magnetic moment with the magnetic field will cause a precession of the spin around the magnetic field. In fact, it is the expectation value of the spin operator that precesses around the magnetic field at a constant frequency known as *Larmor frequency*. This frequency describes the gyration of the spin and is proportional to the magnetic field, thus the name of *gyromagnetic ratio*, g. An additional kinematic effect of precession is introduced due to the acceleration of the relativistic reference frame. This is the case for muons moving at high velocities with a transverse acceleration. This precession is derived in Appendix A and is referred to as *Thomas precession*.

If relativistic muons are constrained to a circular orbit by a uniform magnetic field, as is the case in a *storage ring*[6], their spins experience both Larmor and Thomas precessions. The ensemble of these effects on the spin was worked out by Bargmann, Michel and Telegdi in 1959 [6], in an equation known as the BMT

[6] A storage ring is a circular particle accelerator that maintains particles at the same energy for a long period of time

equation (see Appendix A)

$$\overrightarrow{\omega_s} = \frac{q}{m_\mu c}\left\{\left(a_\mu + \frac{1}{\gamma}\right)\overrightarrow{B} - a_\mu\left(\frac{\gamma}{\gamma+1}\right)\left(\overrightarrow{\beta}\cdot\overrightarrow{B}\right)\overrightarrow{\beta} + \left(a_\mu + \frac{1}{\gamma+1}\right)\overrightarrow{E}\times\overrightarrow{\beta}\right\}, \tag{12}$$

where the velocity is $\overrightarrow{\beta} = \dfrac{\overrightarrow{v}}{c}$, the Lorentz factor is $\gamma = 1/\sqrt{1-\beta^2}$, $\overrightarrow{E}$ and $\overrightarrow{B}$ are the electric and magnetic fields in the laboratory frame respectively. In addition, the muons also travel in a circular orbit with a frequency known as the *cyclotron frequency* (see Appendix A)

$$\overrightarrow{\omega_c} = \frac{q}{\gamma m_\mu c}\left\{\overrightarrow{B} + \frac{\gamma^2}{\gamma^2-1}\left(\overrightarrow{E}\times\overrightarrow{\beta}\right)\right\}. \tag{13}$$

It is convenient to choose a reference frame which rotates with the velocity vector in order to keep the equations simple. In this case, the precession is given by the difference of angular frequencies $\overrightarrow{\omega_a} = \overrightarrow{\omega_s} - \overrightarrow{\omega_c}$,

$$\overrightarrow{\omega_a} = \frac{q}{m_\mu c}\left\{a_\mu\overrightarrow{B} - a_\mu\left(\frac{\gamma}{\gamma+1}\right)\left(\overrightarrow{\beta}\cdot\overrightarrow{B}\right)\overrightarrow{\beta} + \left(a_\mu - \frac{1}{\gamma^2-1}\right)\overrightarrow{E}\times\overrightarrow{\beta}\right\}. \tag{14}$$

If the second and third terms are made to vanish by a proper choice of muon momenta and applied electric and magnetic fields, then Equation (14) becomes

$$\overrightarrow{\omega_a} = a_\mu\frac{q}{m_\mu c}\overrightarrow{B}. \tag{15}$$

In this case, a nonzero a_μ leads to a precession of the muon spin relative to the cyclotron frequency. This is the central equation of the $g-2$ experiment that will be discussed in the next section.

3 Brookhaven $g-2$ Experiment: E821

3.1 Historical Background

The muon magnetic moment has been measured by three consecutive experiments at CERN through the 1960's and 1970's, and a more recent experiment at Brookhaven National Laboratory (BNL), E821. The last CERN experiment developed a number of novel techniques to measure the anomaly. For instance, it employed a storage ring with a transverse uniform magnetic field to extend the muon's lifetime and cancel the second term in Equation (14) since in this case $\overrightarrow{\beta} \cdot \overrightarrow{B} = 0$. The experiment chose a specific momentum according to the relation $a_\mu - 1/(\gamma^2 - 1) = 0$ in Equation (14) known as the *magic momentum*, which causes the spin oscillation to be independent of any applied electric fields. This equation requires the knowledge of the anomaly, which is the quantity the experiment is set to measure. However, the value of the anomaly has already been measured to the first decimal places, which is enough to determine the momentum to the desired precision. The goal of the CERN experiment, on the other hand, was to measure the anomaly to a higher precision. An anomaly value of $a_\mu \approx 1.166 \times 10^{-3}$ led to a Lorentz factor value of $\gamma_{\text{magic}} \approx 29.30$, and thus the magic momentum is approximately 3.09 GeV in the CERN experiment. At the magic momentum, electric quadrupoles[7] were used to provide vertical focusing of the beam. The combined results of the CERN run established a 7.3 ppm precision that was consistent with the standard model prediction. The

[7] An electric quadrupole is a system composed of two pairs of oppositely polarized poles placed antiparallel to each other.

new measurement techniques developed at CERN were used at Brookhaven with some notable improvements such as the higher intensity of the primary proton beam from the proton storage ring; the direct injection of muons into the storage ring instead of pions; the use of kickers to place muons on the correct orbits; the high field uniformity; and the use of Nuclear Magnetic Resonance probes to map the magnetic field distribution. The E821 experiment resulted in a 14-fold improvement over the CERN experiment where it performed four positive muon runs and one negative muon run which gave a combined precision of 0.54 ppm. In this section, a description of the E821 experiment and the summary of its measurements is given.

3.2 Description of the Experimental Method

At BNL, 24 GeV protons are extracted from the proton storage ring AGS (Alternating Gradient Synchrotron) and directed towards a nickel target to generate pions. The pions subsequently decay to muons which pass through selectors that maximize the number of longitudinally polarized muons at the magic momentum of 3.094 GeV/c. These muons are injected into the storage ring via a tangent 1.7 meters long superconducting inflector magnet that provides a 1.5 Tesla vertical field. The field cancels the main storage ring field, allowing the muons to pass almost undeflected into the ring. The muon storage ring has a toroid-shaped structure with a diameter of 14 meters, a beam pipe with a diameter of 90 mm, and a uniform field of 1.45 Tesla. This magnetic field is provided by dipole

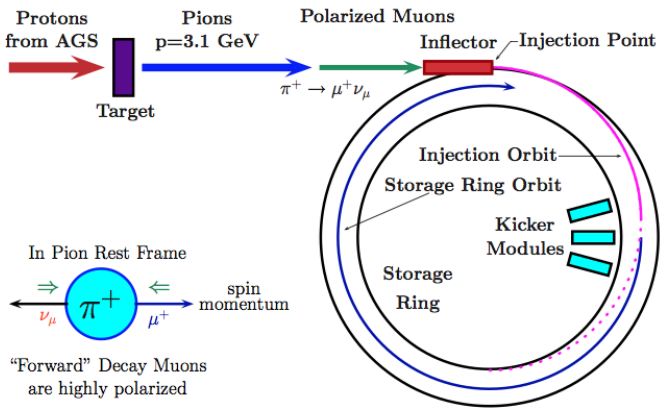

Figure 4: The chain of injection and storage of positive muons in the muon $g-2$ ring at BNL. The "forward" muons refer to muons decaying in the same direction as the laboratory momenta. In this situation, positive muons have their spins anti-parallel to their momenta [3].

magnets[8] that maintain muons in the desired trajectories. However, when the muons are first injected, their trajectories are offset from the storage ring orbit. Pulsed kicker magnets are placed at a specific location in the ring, close to the inflector exit in order to apply a small magnetic field, a "kick," to adjust the orbit by approximately 10 mrad on each injection. Figure 4 shows the complete chain of the muon $g-2$ experiment at BNL for positive muons.

Beam focusing is also needed to constrain the muons within the desired trajectories. Since electric fields do not affect the spin precession, electrostatic quadrupoles are used to continuously focus and defocus the beam in the vertical and the horizontal directions in order to precisely control the beam.

Muons will travel around the ring at the cyclotron angular frequency described

[8] A dipole magnet is a configuration of two opposite pole magnets in the vertical plane of the ring which provide a transverse magnetic field.

by Equation (13), which has a value of approximately 149 ns, and their spin will interact with the magnetic field resulting in a precession with the angular frequency ω_s given by Equation (14). However, the electric field $\overrightarrow{E}$ is negligible ($E \approx 0$) and the uniform magnetic field is transverse ($\overrightarrow{\beta} \cdot \overrightarrow{B} = 0$), so the anomalous precession frequency, $\overrightarrow{\omega_a}$, is given by Equation (15) to the first order. Its magnitude is

$$\omega_a = a_\mu \frac{eB}{m_\mu c} \tag{16}$$

If $g = 2$, then this relative precession ω_a will be zero, which implies that the muon spin is precessing at the same frequency as the cyclotron frequency. On the other hand, if $g \neq 2$, the muon spin will precess at a different rate than the cyclotron frequency, leading the muon spin axis to change by 12 degrees[9] after each rotation for a constant momentum. Figure 5 illustrates this change by showing the momentum vector and the projection of the spin vector in the horizontal plane of the storage ring.

In order to determine the anomaly $a_\mu = \dfrac{g_\mu - 2}{2}$, three quantities need to be determined accurately: ω_a, B, and the muon mass m_μ. The muon mass was determined indirectly by an independent experiment on muonium, the bound state of $\mu^+ e^-$ [7]. The next two subsections describe the measurement of ω_a and the magnetic field B.

[9]The angular change of spin relative to momentum after one revolution around the ring is $\theta_a = \omega_a T_c$. For $a_\mu \approx 1.166 \times 10^{-3}$, $m_\mu = 105.7$ Mev/c^2, $e = 1.6 \times 10^{-19}$ C, and $B = 1.45$ T, $\omega_a \approx 1.45 \times 10^6$ Hz and $T_c \approx 149$ ns, the result using Gaussian units is $\theta_a \approx 12°$.

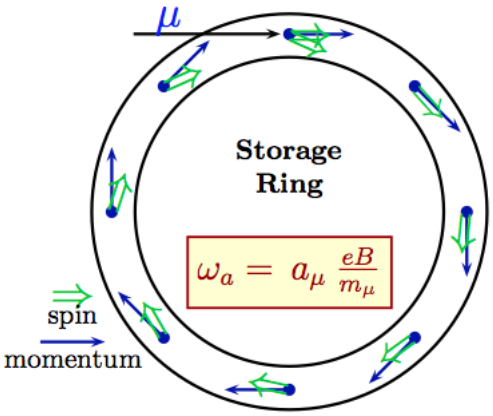

Figure 5: Illustration of the spin precession in the storage ring plane relative to a constant momentum (not to scale). The precession amounts to $\sim$ 12 degrees per orbit [3].

3.3 Measurement of the Anomalous Angular Frequency ω_a

As a result of the muons' high momentum ($\sim$ 3.1 GeV), their lifetime is extended from 2.197 μs at rest to 64.435 μs in the ring. The muons circle the ring many times before they decay into an electron and two neutrinos given by Equation (9). As discussed in Section 2.2, the electron has a preferred emission direction in the muon rest frame that depends on the orientation of the muon spin as given by Equation (10). For example, a positron has a higher probability to be emitted parallel to the muon spin (see Figure 6).

If all decay electrons were detected, the number observed will decay exponentially as $\exp(\frac{-t}{\gamma\tau_\mu})$. Since the interest is in the precession frequency, a choice of a cut on a laboratory observable that directly depends on this frequency is required. A reasonable choice will permit the selection of a subset of the decay electrons in such a way that their number oscillates at the desired frequency ω_a.

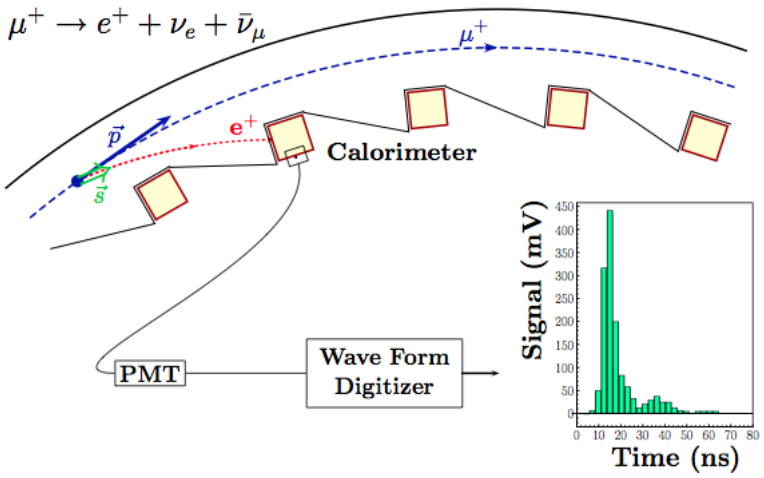

Figure 6: A positive muon in the storage ring emits a positron almost parallel to the muon spin (green arrow). The electron is subjected to the same dipole magnetic field which produces a larger deflection leading the positron to interact with the calorimeter scintillator. The light is detected by a Photomultipler Tube (PMT) generating a signal that is digitized by a Wave Form Digitizer [3].

At the magic momentum $p_\mu \approx 3.09$ GeV/c, the direction of the electrons cannot be chosen as a cut since most decay electrons are nearly parallel to the muon momentum direction, regardless of their decay orientation in the muon rest frame. Instead, a more practical cut can be applied on the electron's laboratory energy. For instance, if only electrons with the highest possible energy are selected, they will represent positrons that decayed nearly parallel to the muon laboratory momentum with maximum muon rest frame energy. The number of these positrons is larger when they are emitted parallel to the muon spin as opposed to when they are antiparallel. So the number of positrons detected will be maximum when the spin is aligned with the decay positron momentum, and will be minimum when the spin is opposite. It becomes clear that the detected electrons will oscillate with the frequency of the muon spin oscillation ω_a.

In practice, the minimum energy threshold is selected to maximize the *statistical figure-of-merit* (FOM), NA^2, in order to minimize the statistical uncertainty. On the left of Figure 7, NA^2 is largest for electrons with $E_{th} \approx 2.6$ GeV ($y \approx .85$). However, the interest is in electrons above an energy threshold. By integrating the quantities N, A, and NA^2 for a single electron threshold as a function of the energy threshold, NA^2 is maximized at $E_{th} \approx 1.8$ GeV as shown on the right of Figure 7.

With the the assumption that the spin precession vector is independent of time, the angle between the spin component in the orbit plane and the muon momentum is $\omega_a t + \phi$, where ϕ is a constant phase. At time t, the number of

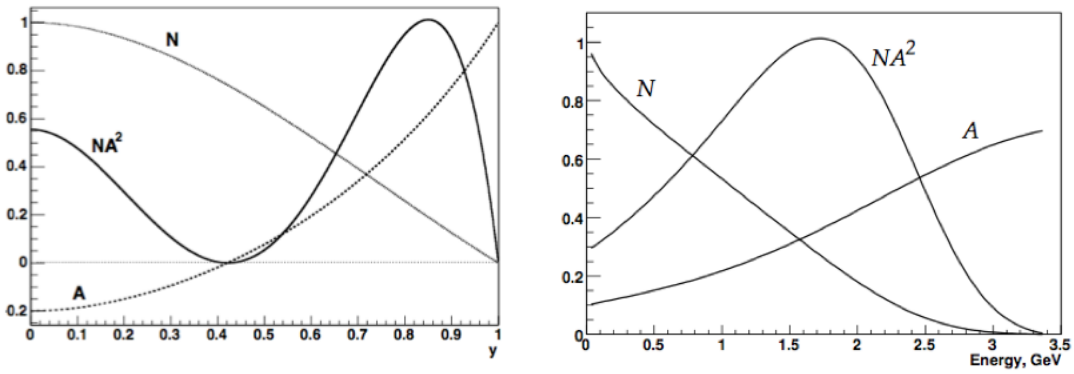

Figure 7: The equivalent of Figure 3 boosted to the laboratory frame. Left: N, A, and NA^2 as a function of the fractional energy $y = E/E_{e,max}$ where $E_{e,max} \approx 3.098$ GeV. Right: Integrated N, A, and NA^2 as a function of the threshold energy [4].

decay positrons N(t) with energy larger than the threshold energy E_{th} is

$$N(t, E_{th}) = N_0(E_{th}) \exp\left(\frac{-t}{\gamma\tau_\mu}\right)\left[1 + A(E_{th}) \sin\left(\omega_a t + \phi(E_{th})\right)\right], \qquad (17)$$

where N_0 is a normalization factor and A is the asymmetry factor for positrons of energy greater than E_{th}. Figure 8 shows the arrival-time spectrum of the final E821 data run for 2001. As discussed earlier, the spectrum follows an exponential decay of the muons modulated by the $g-2$ dependent angular frequency. By fitting this time distribution to the five-parameter function of Equation (17), the angular frequency ω_a is determined.

The electron detection is made via 24 symmetrically distributed calorimeters inside of the ring as shown in Figure 6. The goal of the calorimeters is to determine the electrons' energy and arrival time. The calorimeters are designed to detect the high energy electrons where 65 percent of the electrons with energy higher than

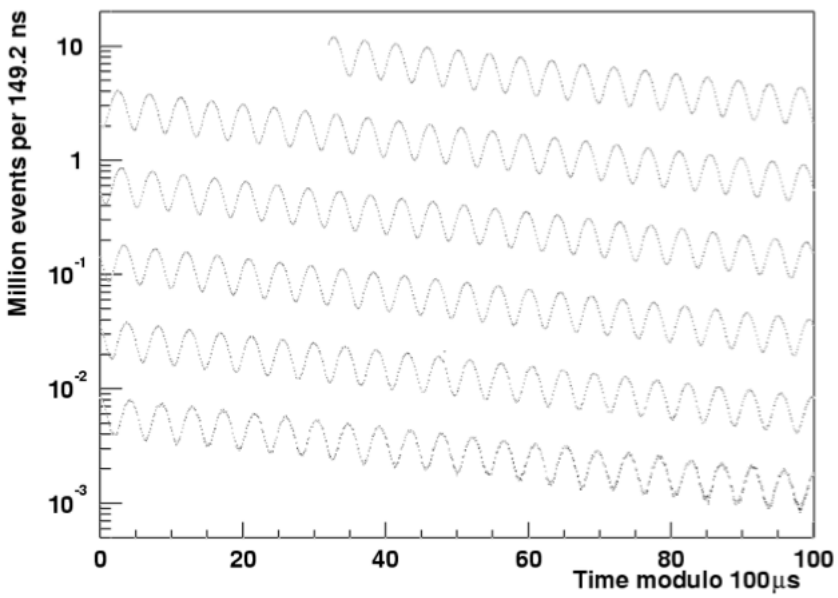

Figure 8: Histogram of the 3.6 billion detected electrons above 1.8 GeV as a function of time, modulo 100 μs, for the 2001 data set [4].

1.8 GeV are intercepted [4]. Each calorimeter is made out of plastic-scintillator[10] material (52% lead alloy, 38% scintillating fiber, and 10% epoxy) read out by photomultiplier tubes[11] (PMTs). The decaying electrons have both tangential and radial momentum components. However, the radial component is quite small, which permits the extrapolation of the electron's trajectory from the calorimeter to the central muon orbit, allowing a measurement of the decay position and vertical angle as shown in Figure 6. The muon position information is particularly important in characterizing the magnetic field felt by the muon at that specific location. Finally, a Wave Form Digitizer (WFD) captures raw analog PMT signals

[10] A plastic-scintillator causes the particle to deposit energy when it passes through. The scintillator re-emits the absorbed energy in the form of light.

[11] Photomultiplier tubes are light detectors that operate via the photoelectric effect where photons, upon hitting a photocathode, generates a cascade of electrons that can be read by a Wave Form Digitizer.

and digitizes them for further processing with the advantage of maintaining high resolution measurements. An example of a WFD output is shown in Figure 6.

3.4 Measurement of the Magnetic Field B

The magnetic field B is weighted by the stored muons distribution and averaged over the running time. It can be expressed as an integral of the product of the muon distribution multiplied by the magnetic field distribution over the storage region leading to a coupling of the moments of the muon distribution to the respective multipoles of the magnetic field. In order to determine the weighted magnetic field B to sub-ppm precision, either the moments and multipoles of the muon and magnetic field distributions should be known extremely well, or a particularly uniform magnetic field and a circular beam aperture is required so that the leading term dominate the multipole expansion of the magnetic field. The latter option was selected where *Nuclear Magnetic Resonance* (NMR) permitted the determination of the magnetic field to the tens of ppb. In this experiment, NMR uses protons in a water sample placed in the dipole magnetic field, and exposed to a $\frac{\pi}{2}$ radio-frequency (RF) pulse which rotates the net magnetization of the protons[12]. A pickup coil placed in the transverse direction registers the induced signal that exponentially decays with an oscillation as the protons' magnetization regains its equilibrium position. This process is known as *Free Induction Decay*, which has a frequency sensitive to the the local magnetic field value. The NMR

[12] A radio-frequency pulse is a pulse in the range from 3 KHz to 300 GHz that excites a large frequency band resulting in the appearance of a time-dependent magnetic field which can rotate the magnetization vector of the protons.

procedure allows the determination of the magnetic field at thousands of points around the ring which permits the mapping and monitoring of the field during data taking. A calibration method is used to express the Larmor spin frequency of a proton in a water sample in terms of the Larmor spin frequency of a free proton ω_p. The latter frequency, ω_p, is related to the magnetic moment of the free proton μ_p and the magnetic field B by [13]

$$B = \frac{\hbar\omega_p}{2\mu_p}. \tag{18}$$

According to the last equation, this weighted magnetic field can be referred to as ω_p. By writing Equation (2) in the form $\frac{q}{mc} = \frac{2\mu_\mu}{1+a_\mu}$ and using Equation (16) and Equation (18), the anomaly can be written in terms of dimensionless ratios,

$$a_\mu = \frac{\mathcal{R}}{\lambda - \mathcal{R}}, \tag{19}$$

where $\lambda \equiv \frac{\mu_\mu}{\mu_p}$ and $\mathcal{R} \equiv \frac{\omega_a}{\omega_p}$. The muon-to-proton magnetic moment ratio, λ, embodies in it both the muon and the proton masses since $\frac{\mu_\mu}{\mu_p} = \frac{g_\mu}{g_p}\frac{m_p}{m_\mu}$. Its value is determined through a precision measurement of the Zeeman ground state hyperfine transitions in muonium (μ^+e^-) by E1054 LAMPF at Los Alamos [7],

$$\lambda_+ = \frac{\mu_{\mu^+}}{\mu_p} = 3.183\,345\,137\,(85).$$

Note that this result has a precision of ~ 27 ppb which could not be obtained by mass measurements. The use of λ_+ to determine a_{μ^-} implies CPT invariance[14].

[13]The Larmor frequency of a free proton is $\omega_p = \gamma_p B$, where γ_p is the free proton gyromagnetic moment ratio given by Equation (2) such that $\overrightarrow{\mu_p} = \gamma_p \overrightarrow{S}$. These relations give the result in Equation (18).

[14]CPT invariance implies that the product of the three discrete transformations C, P, and T taken in any order is a symmetry of theories like the SM. It guarantees that particles and antiparticles have the same masses and lifetimes.

In other words, the relations $a_{\mu^-} = a_{\mu^+}$ and $\lambda_+ = \lambda_-$ must be valid. In fact, the measurement of ω_a for positive and negative muons provides a CPT test where

$$\Delta\mathcal{R} = \mathcal{R}_{\mu^-} - \mathcal{R}_{\mu^+} = (3.6 \pm 3.7) \times 10^{-9}. \tag{20}$$

3.5 Corrections and Systematic Errors

The method described so far presents an ideal scenario. However, there are additional effects that affect the measurements, the most important of which are related to the beam dynamics leading to a displacement of the beam trajectory and the determination of the magnetic field at a location offset from the orbit of the muons. While the dipole magnetic field insures the bending of the muon beam, the vertical focusing is done via electric quadrupoles. These quadrupoles set an electric field gradient that causes the beam to oscillate around its equilibrium in the plane transverse to the beam. This type of oscillation is known as the *betatron oscillation* and it satisfies the harmonic oscillator equations

$$\begin{aligned} \ddot{x} + \omega_x^2 x = 0, \\ \ddot{y} + \omega_y^2 y = 0, \end{aligned} \tag{21}$$

with the frequencies

$$\omega_x = \omega_c\sqrt{1-n}, \qquad \omega_y = \omega_c\sqrt{n}, \tag{22}$$

where ω_c is the cyclotron frequency and n is the field index defined as

$$n = \frac{R_0}{\beta B_0}\frac{\partial E_y}{\partial y}, \tag{23}$$

with an orbit stability condition of $0 < n < 1$ and where R_0 is the equilibrium radius, B_0 is the dipole magnetic field, and β is the muon speed. Since the betatron

frequencies are smaller than the cyclotron frequency, this type of focusing is called *weak focusing*.

The betatron motion perturbs the muon trajectories affecting their momenta and directions. This implies that the assumptions $\overrightarrow{\beta} \cdot \overrightarrow{B} = 0$ and $a_\mu - 1/(\gamma^2 - 1) = 0$ ($E \approx 0$) are no longer valid. These effects should be taken into account in determining the anomalous frequency ω_a as given by Equation (15). The correction for the momentum direction to satisfy $\overrightarrow{\beta} \cdot \overrightarrow{B} = 0$ is called the *Pitch Correction*. Similarly, the momentum spread from the magic momentum requires a correction to the electric field referred to as the *Radial Electric Field Correction*. The combination of these two corrections are explicitly shown in column 4 of Table 3.

Next, the sources of systematic errors in ω_a are briefly defined with their numerical values listed in Table 1:

- Pileup: Two low-energy electrons that reach the detector at very close times can be interpreted as one high-energy electron.

- AGS background: Mis-steering the proton beam in the AGS might lead it to hit a part of the target that produces a higher flux of pions entering the storage ring when muons are injected.

- Lost muons: Small perturbations in the magnetic or electric fields may couple to betatron oscillations at their resonant frequency leading to a motion without bound until the muons are lost.

- Timing shifts and gain changes: A calibration pulse was sent in parallel to the beam data through the optical and electronic readout system to monitor

the time resolution of the detector and variations in the energy scale used.

- Fitting/Binning: The electron decay spectra was sorted into discrete energy bins and fitted to a multi-parameter fitting function for different data subsets which introduced errors related to the corrections applied to the spectra and the experimental conditions.

- Coherent Betatron Oscillation (CBO): Mismatch between the inflector and storage ring apertures at the injection point causes the beam to alternatively widen and narrow as it circulates around the ring.

The systematic uncertainties in the magnetic field measurement are due to effects related to the determination of the precession frequency of protons in a water sample placed in a trolley probe that is offset from the orbit of the muons. The positioning of the trolley permits measurements of the magnetic field during data taking at multiple locations around the ring. However, the magnetic field at the trolley's position might vary from the field that muons experience. In addition, the desired quantity is the free proton precession, but the measured quantity is the proton's precession in water. For these reasons, uncertainties are introduced in the processes of calibration and interpolation. Table 2 summarizes the numerical values of the errors in ω_p for three running periods.

The electric dipole moment (EDM) of the muons should also be mentioned for completeness of the discussion. Just as the magnetic moment originates from the current of the spinning charged lepton and interacts with the magnetic field, the EDM is due to the electric charge of the spinning lepton and it interacts with the

Table 1: Systematic errors for ω_a for the three high-statistics running periods. † In the 2001 run, the AGS background, timing shifts, E field and pitch correction, binning and fitting procedure have a total systematic error of 0.11ppm.

Years	1999 (ppm)	2000 (ppm)	2001 (ppm)
Pileup	0.13	0.13	0.08
AGS background	0.10	0.01	†
Lost Muons	0.10	0.10	0.09
Timing Shifts	0.10	0.02	†
E-field and pitch	0.08	0.03	†
Fitting/Binning	0.07	0.06	†
CBO	0.05	0.21	0.07
Gain Changes	0.02	0.13	0.12
Total systematic error on ω_a	0.3	0.31	0.21

Table 2: Systematic errors for ω_p for the three high-statistics running periods. † After 1999, the inflector, which was damaged, was replaced making the disturbance of the inflector's fringe field on the main storage ring field negligible.

Years	1999 (ppm)	2000 (ppm)	2001 (ppm)
Absolute calibration of standard probe	0.05	0.05	0.05
Calibration of the trolley probes	0.20	0.15	0.09
Trolley measurements of B	0.10	0.10	0.05
Interpolation with fixed probes	0.15	0.10	0.07
Uncertainty from muon distribution	0.12	0.03	0.03
Inflector fringe field uncertainty	0.20	†	†
Others	0.15	0.10	0.10
Total systematic error on ω_p	0.4	0.24	0.17

electric field. The equivalent of Equation (2) for an EDM is

$$\overrightarrow{d} = \eta \frac{q}{2mc} \overrightarrow{S} \tag{24}$$

where d is the dimensionless constant equivalent to the g-factor. Equation (19) assumes a zero muon EDM. For a non-zero muon EDM, the spin frequency is

$$\overrightarrow{\omega} = \overrightarrow{\omega}_a + \overrightarrow{\omega}_{EDM} = \overrightarrow{\omega_a} - \frac{q\eta}{2m} \left(\overrightarrow{\beta} \times \overrightarrow{B} \right) \tag{25}$$

However, the current experimental value for muons EDM is $d_\mu = (-0.1 \pm 0.9) \times 10^{-19} e \cdot \text{cm}$ [2], which is too small to affect the anomalous precession frequency ω_a.

3.6 Summary of Results from E821

E821 has conducted four positive muon runs (1997-2000) and one negative muon run (2001) that are all reported in [4]. The results of the experiment for the last three runs are displayed in Table 3 and Table 4.

The averaged value of the ratio $\mathcal{R} = \omega_a/\omega_p$ of Equation (19) evaluated in the cases of negative and positive muons is

$$\mathcal{R}_\mu \, (\text{E821}) = 0.003\,707\,206\,4(20). \tag{26}$$

The anomalous magnetic moment is thus

$$a_\mu^{\text{E821}} = 11\,659\,208\,(5.4)_{stat}\,(3.3)_{sys}\,(6.3)_{tot} \times 10^{-10} \quad (0.54 \text{ ppm}) \tag{27}$$

This final measurement has a statistical uncertainty of 0.46 ppm and a systematic uncertainty of 0.28 ppm which were added in quadrature to get a total uncertainty of 0.54 ppm. In order to improve the statistical uncertainty to the same level as

Table 3: Results for the anomalous precession frequency ω_a including the relative electric field and pitch corrections shown in column 4 and the event-weighted magnetic field ω_p given with their uncertainties. The error on the average takes into account the correlated systematic uncertainties between different periods.

Years	Electrons [millions]	$\omega_a/(2\pi)$ [Hz]	E/pitch [ppm]	$\omega_p/(2\pi)$	$\mathcal{R} = \omega_a/\omega_p$
1999 (μ^+)	950	229 072.8(3)	0.81(8)	61 791 256(25)	0.003 707 204 1(51)
2000 (μ^+)	4000	229 074.11(16)	0.76(3)	61 791 595(15)	0.003 707 205 0(25)
2001 (μ^-)	3600	229 073.59(16)	0.77(6)	61 791 400(11)	0.003 707 208 3(26)
Average					0.003 707 206 3(20)

Table 4: BNL E821 results of the anomaly a_μ for the three high-statistics running periods.

Years	Polarity	$a_\mu \times 10^{10}$	Precision [ppm]
1999	μ^+	11 659 202(15)	1.3
2000	μ^+	11 659 204(9)	0.73
2001	μ^-	11 659 214(9)	0.72
Average		11 659 208.0(6.3)	0.54

the systematic uncertainty, an additional running period of 8 years is required. Alternatively, the experiment can use a higher intensity beam to produce more electrons, and thus more statistics. This is precisely what the new Fermilab experiment does.

4 Future Fermilab $g-2$ Experiment: E989

The Fermilab experiment, E989, will measure the anomaly a_μ with an error of 1.6×10^{-10} leading to a fractional error of 0.14 ppm, where the level of the statistical and systematic uncertainties are both at the 0.10 ppm level. In order to achieve this goal, a collection of data that is twenty-one times larger than the E821 data collection is required, which scales to 1.8×10^{11} detected positrons with energy greater than 1.8 GeV, and arrival time greater than 30 μs after muon injection in the storage ring. Since the detected positron number is directly proportional to the protons on target, the Fermilab experiment will have to deliver 4×10^{20} protons. Indeed, it will be possible to reach these numbers by using the Fermilab beam complex which is expected to annually deliver 2.3×10^{20} 8 GeV protons on an Inconel[15] core target. At this rate, the desired number of protons, and thus positrons, will be achieved in less than two years of running.

Fermilab will improve upon the methods and instrumentation used at BNL. For instance, the produced pion beam will pass through a bending magnet to select particles with a momentum of 3.1 GeV ($\pm$ 10 %), and subsequently traverse

[15]Inconel is an alloy, composed of a metal and other elements, specifically designed to withstand high beam stresses.

a decay line of over one kilometer, which results in a pure muon beam entering the storage ring. The muon storage ring will be filled at a repetition rate of 15 Hz compared to 4.4 Hz at BNL, and the stored muon-per-proton ratio will also be increased by a factor of 5 to 10 times. The muons will enter the ring via a new superconducting inflector, characterized by a limited flux leakage onto the storage region and a larger horizontal beam aperture to allow a higher storage efficiency. The muon kicker will have an optimized pulse-forming network[16] that will provide a pulse close to the beam width, as opposed to the E821 kicker which had a pulse width longer than the cyclotron period. At BNL, the injected muon beam was contaminated with pions which introduced a hadronic flash background. This background will be reduced by a factor of 20 in E989.

E989 will use the same muon storage ring of E821, which has been relocated to Fermilab in the summer of 2013 in a new building characterized by mechanical stability and controlled temperature. These options were not available at BNL.

The new segmented calorimeters will use silicon Photomultipliers (SiPMs) to read signals from lead-fluoride crystal (PbF_2). The crystal has an improved energy resolution and a very fast Cherenkov signal[17] response. When a photon strike a SiPM pixel, it generates an avalanche that is linearly combined with the other pixels that were hit to form the response. SiPMs are designed so that their number of pixels exceed the number of photons that are expected to strike

[16] A pulse-forming network is an electric circuit composed of capacitors that provide a square pulse with a flat top upon discharge.

[17] A Cherenkov signal is due to Cherenkov radiation which is an electromagnetic radiation produced when a particle travel through a dielectric material with a velocity greater than the phase velocity of light in that dielectric. While no particle travels faster than light in vacuum, the situation is different in a dielectric since $v_{\text{light}} = c/n$ with $n > 1$.

the device allowing a high photo-detection efficiency. The added benefit of using SiPMs is that they can be placed inside the storage ring at the back of the PbF_2 crystals without perturbing the field, as opposed to PMTs which require long lightguides.

Since momentum spread, betatron oscillations, and muons distribution introduced ppm level corrections in the anomalous precession at BNL, E989 introduces in-vacuum straw drift tubes[18] as tracking detectors to better understand beam dynamics, limit pile up effects, and provide an independent validation of the systematic uncertainties analysis (for example, an independent momentum measurement.) In addition, it will also be used to search for a permanent EDM. The electronics and data acquisition systems will be upgraded to handle the increased rate of data taking and to record all information related to the run for monitoring and the application of corrections in the analysis stage.

Last but not least, the storage ring magnetic field, and thus ω_p, will be measured with an uncertainty that is approximately 2.5 times smaller by placing critical NMR probes at strategic locations around the ring and shimming the magnetic field to achieve a high uniformity in addition to other incremental adjustments. Tables 5 and 6 compare the systematic uncertainties in ω_a and ω_p as obtained by BNL E821 and as planned for FNAL E989 experiments [8].

[18] A straw tube for high resolution position measurement is constructed with an anode wire centered within a cathode tube and maintained at a potential difference in a gas environment. When a charged particle passes through the tube, it ionizes the gas generating a signal for a particle "hit".

Table 5: Comparison of systematic errors for ω_a between BNL E821 and FNAL E989.

Category	E821 (2001) (ppm)	E989 Goal (ppm)
Pileup	0.08	0.04
Lost Muons	0.09	0.02
E-field and pitch	0.05	0.03
CBO	0.07	< 0.03
Gain Changes	0.12	0.02
Total systematic error on ω_a	0.18	0.07

5 The Standard Model Evaluation of the Anomaly (a_μ)

5.1 Introduction

The magnetic moment of the muon is described by Equation (2)

$$\overrightarrow{\mu} = g\frac{q}{2mc}\overrightarrow{S}, \qquad g = 2\left(1 + a_\mu\right), \tag{28}$$

where $g = 2$ in the Dirac theory. Particles with $g = 2$ are referred to as Dirac particles. The anomaly a_μ is due to quantum fluctuations that couple the muon spin to virtual fields which leads to contributions that can be calculated in the SM theory. For instance, the three interactions that the SM describes are electromagnetic interactions by Quantum Electrodynamics (QED), hadronic strong interactions by Quantum Chromodynamics (QCD), and weak interactions by the Electro-Weak theory (EWT). In this language, the anomaly can be written

Table 6: Comparison of systematic errors for ω_p between BNL E821 and FNAL E989.

Category	E821 (2001) (ppm)	E989 Goal (ppm)
Absolute calibration of standard probe	0.05	0.035
Calibration of the trolley probes	0.09	0.03
Trolley measurements of B	0.05	0.03
Interpolation with fixed probes	0.07	0.03
Uncertainty from muon distribution	0.03	0.03
Time dependent external B fields	—	0.005
Others	0.10	0.03
Total systematic error on ω_p	0.17	0.070

as the sum of contributions from each theory as

$$a_\mu^{SM} = a_\mu^{\text{QED}} + a_\mu^{\text{Hadronic}} + a_\mu^{\text{EW}}. \tag{29}$$

The QED and weak contributions to the anomaly are well understood and have been evaluated using perturbation theory to a high precision leading to small errors, and thus permitting the comparison with experimental results. On the other hand, the hadronic contribution limits the accuracy of the theoretical prediction since these effects cannot be evaluated using perturbation methods at low energies. For this reason, the hadronic contribution has to be evaluated using experimental data via a dispersion relation, and thus leading to the highest uncertainty in the prediction.

5.2 The QED Contribution to a_μ

The mediator of electromagnetic processes that involves the interactions between charged particles is the photon. In a loose language, sometimes the muon will "recapture" the photon it emitted and thus forming a new "Dirac muon + photon" system.If the magnetic moment of the muon is probed at that instant, it will be different than 2 since the configuration does not have just a Dirac muon. Similarly, there can be more than one photon or even electron-positron pairs that form a new system, and thus the contributions to g of Equation (28) can be expressed as a series in the form: Dirac muon + {Dirac muon + photon} + {Dirac muon + several photons} + {electron + positron} ....

Formally, the dominant contribution is that of the lowest-order (LO) QED

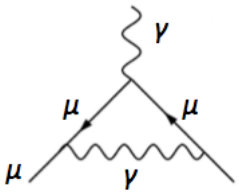

Figure 9: The lowest-order (Schwinger) contribution to the muon magnetic moment anomaly [10].

process that involves the exchange of a virtual photon and is represented by a one-loop diagram as illustrated in Figure 9. This contribution is known as the *Schwinger term* and it is common to all three charged leptons. Its value is calculated in Appendix C and the result is

$$a_\mu^{\mathrm{QED,LO}} = \frac{\alpha}{2\pi} \approx 1.16 \times 10^{-3}, \tag{30}$$

where α is the fine structure constant that has been measured experimentally in the ^{87}Rb atom with 0.66 ppb precision and has an inverse value of

$$\alpha^{-1}\,(\mathrm{Rb}) = 137.035\,999\,049(90)\ [9]. \tag{31}$$

Equation (28) can be written to first order in α representing the first-order term in the one-loop diagram contribution

$$g = 2\left(1 + \frac{1}{2}\frac{\alpha}{\pi} + \mathcal{O}\left(\left(\frac{\alpha}{\pi}\right)^2\right)\right), \tag{32}$$

where the higher-order corrections to QED processes are suppressed by increasing powers of α. In fact, the QED calculation has been carried out to the fifth-loop contribution

$$a_\mu^{\mathrm{QED}} = 116\,584\,71.895\ (0.009)(0.019)(0.007)(0.077) \times 10^{-10}\ [11] \tag{33}$$

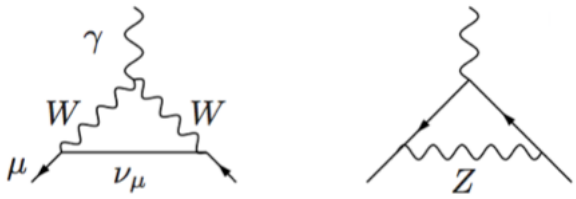

Figure 10: Weak contributions to the muon anomalous magnetic moment with a one-loop diagrams with virtual W and Z gauge bosons [10].

with the uncertainties corresponding to the lepton mass ratios, the eight-order term in the four-loop contribution, the tenth-order term in the five-loop contribution, and the value of the fine structure constant $\alpha\,(\mathrm{Rb})$. It should be noted that this contribution accounts for over 99.99% of the total contribution to the muon magnetic moment anomaly with much smaller uncertainties than the experimental value.

5.3 The Weak Contribution to a_μ

The weak contribution is the smallest correction to the anomaly. The current electroweak calculation is performed up to two loops. The leading electroweak effect originates from the single loop diagrams of Z and $\mathrm{W}^{\pm}$ bosons shown in Figure 10 with a result of

$$a_\mu^{\mathrm{EW}(1)} = 19.48 \times 10^{-10}\ [12]. \tag{34}$$

The two-loop contribution is negative which reduces the weak contribution, and

Figure 11: The Feynman diagrams for the three different hadronic contributions to a_μ [10].

the third-loop contribution is negligible leading to a total result of

$$a_\mu^{\mathrm{EW}} = 15.36(1.0) \times 10^{-10} \text{ [13]}, \tag{35}$$

where the error is due to unknown higher order contributions. Nevertheless, the error is very small. Since the weak contribution to the anomaly is of the order of 1.3 ppm, the 0.54 ppm precision of E821 allowed this experiment to be the first to probe the weak scale of the SM and subsequently test a_μ^{EW}.

5.4 The Hadronic Contribution to a_μ

The hadronic contribution is the second largest contribution, which constitutes about 60 ppm of the total value of a_μ with a dominant error of about 0.4 ppm. This contribution is divided into three pieces: the leading order (LO) and higher order (HO) vacuum polarization (VP) contributions, and the light-by-light (LbL) scattering contribution. Hence, a_μ^{Had} can be expressed as

$$a_\mu^{\mathrm{Had}} = a_\mu^{\mathrm{Had,LOVP}} + a_\mu^{\mathrm{Had,HOVP}} + a_\mu^{\mathrm{LbL}}. \tag{36}$$

Schematics of these three contributions are shown in Figure 11.

VP refers to the partial screening of the charge of a particle by the vacuum which plays the role of a dielectric medium. In the case of the hadronic contri-

bution to the muon anomaly, the virtual photon of Figure 9 may lead to the virtual creation and re-absorption of quark pairs and the corresponding hadrons, schematically represented in Figure 11 by "had." corresponding to all possible hadronic states. While electromagnetic and weak interactions have small values for their coupling constants allowing perturbative expansions in these constants, the strong interactions have a small coupling only at high energies preventing the use of perturbative methods at low energies. Generally, the energy region below 2 GeV cannot be treated using perturbative QCD. The virtual hadrons that affect the anomaly have an energy scale of $m_\mu c^2 \approx 106$ MeV which is well below the perturbative QCD region. For this reason, a semi-phenomenological method that uses experimental input from hadronic e^+e^- annihilation data to evaluate the LO and HO VP contributions is employed. The method, known as the dispersion relation, relates the photon VP due to hadronic contributions shown in the two left diagrams in Figure 11 to the total $e^+e^- \rightarrow$ hadrons cross section at low energies which is obtained from experimental data. The improvement in the measurement of e^+e^- annihilation to hadrons at low energies have been the focus of several experiments. Some of the experiments are CMD2 and SND collaborations in Novosibirsk (Russia); the KLOE collaboration at Frascati (Italy); and the BaBar at SLAC (USA). It should be noted that there is an alternative method in evaluating the VP contributions by using the τ-decays. However, the obtained result is problematic as it differs from the e^+e^- results as shown in Figure 12 (Davier et al., τ10). One of the most recently reported LO hadronic

contribution is

$$a_\mu^{\text{Had,LOVP}} = 6\,94.9(43) \times 10^{-10}\ [5]. \tag{37}$$

While the HO hadronic contribution is given by

$$a_\mu^{\text{Had,HOVP}} = -9.84(0.7) \times 10^{-10}\ [5]. \tag{38}$$

The hadronic LbL contribution, shown in the far right schematic of Figure 11, is of the order of $\mathcal{O}\left(\alpha_s^3\right)$ which is quite small. Since the process involves three virtual photons, the use of experimental data to evaluate the LbL contribution is not possible. Instead, the contribution is evaluated based on hadronic models with the requirement that they correctly reproduce the QCD properties. The downside of this approach is that the final result is model dependent. Currently, active research work is being done in this area. One of the calculations obtained is

$$a_\mu^{\text{Had,LbL}} = 10.5(26) \times 10^{-10}\ [14]. \tag{39}$$

5.5 The SM Value of a_μ

The SM is determined using the QED contribution given in Equation (33) from [11], the EW contribution given in Equation (35) from [13], the hadronic LbL contribution given in Equation (39) from [14], the LO VP given in Equation (37) from [5], and finally the HO VP given in Equation (38) from [5]. The final result is:

$$a_\mu^{SM} = (116\,591\,82.8 \pm 4.5) \times 10^{-10}\,(0.39\ \text{ppm})\ \ [5]. \tag{40}$$

There are several groups that evaluated the anomaly, so the above result is not the only one. Except for one group, all the other evaluations have values close

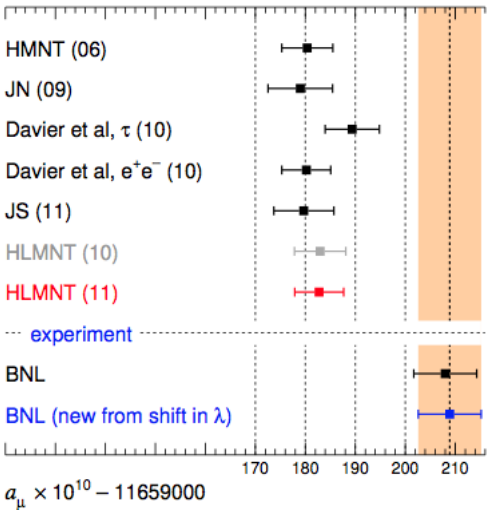

Figure 12: SM predictions of a_μ calculated by several groups. The new experimental result is due to an improvement in the measurement of the muon-to-proton magnetic moment ratio λ [5].

to each other and approximately three standard deviations away from the BNL result as illustrated in Figure 12.

The present error in the SM determination of the anomaly a_μ is dominated by the errors in the LO VP and LbL contributions, 4.3 $\times 10^{-10}$ and 2.6 $\times 10^{-10}$ respectively. The error in the LO VP is expected to diminish to 2.6 $\times 10^{-10}$ by the expected new data from new collaborations such as VEPP-2000 in Novosibirsk and BES-III at BEPC (China). The projected combined error of LO VP and LbL could go down to 3.0 $\times 10^{-10}$ [15]. By combining the proposed Fermilab error of 1.6 $\times 10^{-10}$ with the new expected theoretical error, the total error in the difference between experiment and theory could go down to 3.1 $\times 10^{-11}$, to be compared with the current 7.7 $\times 10^{-11}$. By assuming that the experimental and theoretical values of the anomaly do not change, the new deviation is at the 8.1σ

level. This last result is an important motivation for the continuous efforts in improving the experimental and theoretical determinations of the muon magnetic moment anomaly.

6 Conclusions and Prospects

The SM calculation of the anomalous magnetic moment of the muon is smaller than the recent experimental measurement performed by BNL. Depending on the SM evaluation, the discrepancy is approximately $\Delta a_\mu\,(\mathrm{E821} - \mathrm{SM}) = (25.2 \pm 7.7) \times 10^{-10}$, which is larger than the 3σ level. This difference will be investigated by a future FNAL experiment which aims at reducing the error in the measurement to $1.6{\times}10^{-10}$. In parallel, theoretical groups aim at reducing the SM error to $3.0\ {\times}10^{-10}$.

Currently, candidates such as supersymmetry, extra dimensions, and dark matter models attempt to account for the discrepancy. On the high energy frontier, the LHC is sensitive to the electroweak symmetry breaking (EWSB) scale and its extension that may incorporate new particles and new interactions from the above models. While the first run of the LHC has concluded with the discovery of a new particle compatible with the SM Higgs boson, new physics beyond the SM has not yet been found. The new 2015 run of the LHC is expected to collect a significantly large amount of data at $\sqrt{s} = 13$ TeV, and thus probe the weak-scale extensions of the SM. However, even if the LHC discovers new effects, it is still not in its capacity to discern between the possible interpretations of different models.

In other words, the LHC data might be compatible with different models leading to alternative explanations. For this reason, the LHC requires complementary experiments to determine the properties of any possible new physics. The muon $g-2$ is one of the experiments that is sensitive to parameters not accessible to the LHC. The evaluation of the anomaly is affected by a large class of models describing the TeV scale that may be used to constrain the parameter search at the LHC.

In short, the muon $g-2$ magnetic moment anomaly is sensitive to SM physics and beyond which is valuable in complementing searches at the LHC, and at the same time constraining existent and future theoretical models. While the discrepancy between experiment and theory has yet to be confirmed with the new FNAL experiment, and more data at higher energy needs to be collected by the LHC to search for new physics, the muon $g-2$ remains an important tool to explore physics beyond the standard model at the TeV scale.

References

[1] F. Jegerlehner, *The Anomalous Magnetic Moment of the Muon* (Springer Berlin Heidelberg, Berlin, 2008).

[2] J. Beringer et al., Phys.Rev. **D86**, 010001 (2012).

[3] F. Jegerlehner and A. Nyffeler, arXiv:0902.3360v1 (2009).

[4] G. W. Bennett et al., Phys. Rev. D **73**, 072003 (2006).

[5] K. Hagiwara, R. Liao, A. D. Martin, D. Nomura, and T. Teubner, J.Phys. **G38**, 085003 (2011).

[6] V. Bargmann, L. Michel, and V. Telegdi, Phys.Rev.Lett. **2**, 435 (1959).

[7] W. Liu et al., Phys. Rev. Lett. **82**, 711 (1999).

[8] R. Carey et al., FERMILAB-PROPOSAL-0989 (2009).

[9] R. Bouchendira, P. Clade, S. Guellati-Khelifa, F. Nez, and F. Biraben, Phys. Rev. Lett. **106**, 080801 (2011).

[10] R. Liao, Ph.D. thesis, University of Liverpool, 2011.

[11] T. Aoyama, M. Hayakawa, T. Kinoshita, and M. Nio, Phys.Rev.Lett. **109**, 111808 (2012).

[12] F. Jegerlehner and A. Nyffeler, Phys.Rept. **477**, 1 (2009).

[13] C. Gnendiger, D. Stckinger, and H. Stckinger-Kim, Phys.Rev. **D88**, 053005 (2013).

[14] J. Prades, E. de Rafael, and A. Vainshtein, arXiv:0901.0306 (2009).

[15] T. Blum et al., arXiv:1311.2198 (2013).

Appendix A

Spin Dynamics

Appendix B

Muon Decay Rate

Appendix C

Radiative Corrections